Iraqi Journal of Physics, 2025 *Vol.23, No.1, PP.20-30*
https://doi.org/10.30723/ijp.v23i1.1311 *P-ISSN: 2070-4003*
E-ISSN: 2664-5548

Charge Density Distributions, Elastic and Inelastic Electron Scattering Form Factors of ^{20}Ne and ^{24}Mg Nuclei

Hassan K. Issa[1a*] and Ghaith N. Flaiyh[1b]
[1]*Department of Physics, College of Science, University of Baghdad, Baghdad, Iraq*
[a*]Corresponding author: hassan.kalid@sc.uobaghdad.edu.iq

Abstract
In this study, the charge density distribution was calculated using the folding model, which has been applied to study the roles upon the center of mass and Pauli pair association affect the density relying on the efficient two-body interactions, as a formula for the two-body density applicable to limit nuclei may be derived in terms of the pair correlation function for ^{20}Ne and ^{24}Mg nuclei. The elastic electrons scattering form factors F(q) and the root of the mean square charge radii $\langle r^2 \rangle^{1/2}$were determined. The inelastic longitudinal electron scattering form factors associated with the isosceles transitioning T = 0 of the($J_i^\pi \rightarrow J_f^\pi$): ($0^+ \rightarrow 2^+$) and ($0^+ \rightarrow 4^+$) for the ^{20}Ne and ^{24}Mg nuclei were determined. A wave function within the model space, which is defined by the orbits $1d_{5/2}$, $2s_{1/2}$ and $1d_{3/2}$, is unable to produce an acceptable form factor. Using the folding model to estimate the lower state form for distribution of charge density and adopting the shape of the Tassie model, the core polarization transition density is calculated. An astounding understanding of the computed inelastic longitudinal F(q)'s and those of observational data is seen for all investigated nuclei, and it is noted that the core polarization effects, which reflect the group modes, are crucial to this outcome.

Article Info.

Keywords:
Charges Density, Elastic Electrons Scattering, Inelastic Electrons Scattering, Folding Model, Tassie-Model.

Article history:
Received: Jun. 05, 2024
Revised: Oct. 01, 2024
Accepted: Oct. 06, 2024
Published: Mar. 01,2025

1. Introduction
Electron scattering is the consequence of an electromagnetic reaction. There are many theories on why an electron is such an effective instrument for studying the structure of nuclear particles [1, 2]. The electron's fundamental attachment to the object being targeted nucleus is well-established. It is feasible to conduct measures on the targeted nucleus without substantially altering its structure as a result of the relatively weak interaction. In contrast, the target's shape and relationship with nuclear particles are not known, which makes it very difficult to distinguish between them during the examination of the results of experiments. The effect of the electron scattering operator instantly links its cross-section to the change in matrix components of the localized charged and current-density operator, which in turn is directly related to the target nucleus's structure [3].

Radhi et al. [4] have studied the nuclear structure of ^{19}F nucleus, inelastic electron scattering form factors, energy levels and transition probabilities for positive and negative low-lying states. Mahmood and Flaiyh [5, 6] have employed an effective two-body density operator for a point nucleon system folded with the tensor force correlations. The operator has been used to derive an explicit form for the ground state two-body charge density distribution (2BCDD) applicable for some light nuclei. Sarriguren and Merino [7] have studied the magnetic form factors corresponding to elastic electron scattering from odd-A nuclei. The calculations are carried out in plane-wave Born approximation. Al-Rahmani et al. [8] have studied the short-range effects on C2 and C3; they also examined C4 form factors in the ^{26}Mg nucleus. Flaiyh and Sharrad [9] have studied “the effective two-body density operator for a point nucleon system folded with the full two-body correlations (which include the tensor correlations and short-range correlations)”.

In this work, distribution of charge density, elastic and inelastic form factors of ^{20}Ne and ^{24}Mg target nuclei were calculated. It is currently acknowledged that the description of electron scattering data is inadequate when form factors are calculated exclusively using the extensive particle shell model space by comparing theoretical results with experimental results. Therefore, it is imperative to include the effects of the two-body effective folding model (core polarization) in the equations. This phenomenon can be explained by the polarization of core protons (p) by the surrounding protons (p) and neutrons (n). The Tassie model [10] provides the shape of the transition density for the excitation in question. This model, when coupled with the two-body charge density distribution and simple shell model predictions, results in a high degree of accord in the evaluated and experimental data for the longitudinal structure factors of elastic and inelastic materials during transitions J_i T_i = 0+ 0 to J_f T_f = 2^+ 0 and 4^+ 0 for ^{20}Ne and ^{24}Mg nuclei.

2. Theoretical

The operator in the following defines the charge density of nuclei composed of A-particles that are shaped like points [11]:

$$\rho_{ch}^{(1)}(r) = \frac{1}{4\pi}\sum_{n\ell j} \eta_{n\ell j}(2j+1)|R_{n\ell}(r)|^2 \qquad (\mathbf{1})$$

where the state's livelihood percentage is represented by the parameter η_{nlj}, $R_{nl}(r)$ is the harmonic oscillator radial wave function and (2j+1) is the occupation number of sub–orbits. The folding model was discovered and realized as highly beneficial for the phenomenology examination of nucleon-nucleus scattering results in relation to the ground state density of the objective and a two-body effective interaction [12]. The objective density was considered to be unrelated to the effective interaction in the model's initial applications. The pair correlation function can be used to determine an equation of the density of two-body operators that are suitable for finite nuclei based on the following relation:

$$\rho^{(2)}{}_{(\vec{r}1,\vec{r}2)} = \rho^{(1)}(r_1)\rho^{(1)}(r_2) + C(\vec{r}_1,\vec{r}_2) \qquad (\mathbf{2})$$

$C(\vec{r}_1,\vec{r}_2)$ is the center of mass (c.m.) and C_{cm} and C_p are the Pauli pair correlation functions [13], So that:

$$C(\vec{r}_1,\vec{r}_2) \cong C_{c.m.}(\vec{r}_1,\vec{r}_2) + C_p(\vec{r}_1,\vec{r}_2) \qquad (\mathbf{3})$$

where:

$$C_{c.m.}(\vec{r}_1,\vec{r}_2) = \frac{r_1.r_2}{2A\alpha^2}\left(\frac{1}{r_1}\frac{d\rho_1}{dr_1}\right)\left(\frac{1}{r_2}\frac{d\rho_1}{dr_1}\right) \qquad (\mathbf{4})$$

$$C_p(\vec{r}_1,\vec{r}_2) \cong \frac{1}{A-1}\left[1 - \frac{c_0}{A-1}e^{\frac{k_f^2}{5}|\vec{r}_1-\vec{r}_2|}\right]\rho^{(1)}{}_{(\vec{r}_1)}\rho^{(1)}{}_{(\vec{r}_2)} \qquad (\mathbf{5})$$

Substituting Eq.s (4) and (5) into Eq. (3) and using Eq. (3) in Eq. (2), we get:

$$\rho^{(2)}{}_{(\vec{r}1,\vec{r}2)} = \rho^{(1)}{}_{(\vec{r}1)}\rho^{(1)}{}_{(\vec{r}2)} + \frac{r_1.r_2}{2A\alpha^2}\left(\frac{1}{r_1}\frac{d\rho_1}{dr_1}\right)\left(\frac{1}{r_2}\frac{d\rho_1}{dr_1}\right) + \frac{1}{A-1}\left[1-\frac{c_0}{A-1}e^{\frac{k_f^2}{5}|\vec{r}1-\vec{r}2|}\right] \quad \textbf{(6)}$$

$$\rho^{(1)}(\vec{r}_1)\ \rho^{(1)}(\vec{r}_2)$$

where $c_0=3(\pi/5)^{1/2}$, α is the oscillator constant $\left(\alpha^2 = 0.99\,A^{-1/3}\right)$ and K_f is the local Fermi momentum.

The ground state two-body distribution of charge-density $\rho_{ch}^{(2)}(r)$ is provided by the expected result of the functional two-body distribution of charge-density generator in E. (6) stated as:

$$\rho_{ch}^{(2)}(r) = \sum_{i<j}\langle ij|\,\rho^{(2)}_{(r_i,r_j)}[|ij\rangle - |ji\rangle] \qquad (\textbf{7})$$

where $|ij\rangle$ is the two particle wave function. The nuclei mean square charge radius is:

$$\langle r^2\rangle^{1/2} = \frac{4\pi}{z}\int_0^\infty \rho_{ch}(r)r^4dr \qquad (\textbf{8})$$

The ground state distribution of charge density can be utilized in the computation method of the elastic electron scattering form factor from spin 0 nuclei (J=0). All coming and scattered waves of electrons are regarded as plane waves in the Plane Wave Born Approximation (PWBA), and the ground state distribution of charge density is spherically symmetric and real. Consequently, the form of the factor is the Fourier transform of the ground state distribution of charge density. Thus [14, 15]:

$$F(q) = \frac{4\pi}{Z}\int_0^\infty \rho_o(r)\,j_0(qr)r^2dr \qquad (\textbf{9})$$

where $\rho_o(r)$ is the ground state two-body charge density distribution represented in Eq. (7), $j_0(qr) = \sin(qr)\ /(qr)$ is the momentum transfer from the incident electron to the target nucleus, and is the zeroth order of the spherical Bessel function. It is possible to express Eq. (9) as:

$$F(q) = \frac{4\pi}{qZ}\int_0^\infty \rho_o(r)\sin(qr)rdr \qquad (\textbf{10})$$

The form factors of inelastic longitudinal electrons scattering, which entail angular momentum J and momentum transition(q), are expressed as [10]:

$$\left|F_J^L(q)\right|^2 = \frac{4\pi}{Z^2(2J_i+1)}\left|\ \langle f\|\widehat{T}_J^L(q)\|i\rangle\ \right|^2|F_{cm}(q)|^2|F_{fs}(q)|^2 \qquad (\textbf{11})$$

where $\widehat{T}_J^L(q)$ is the longitudinal electrons scattering generator. Consequently, it is possible to express the form factors of Eq. (11) in the form of matrix elements that are decreased in both angular momentum and isospin, as the nuclear states have established isospin $T_{i/f}$ [16]:

$$\left|F_J^L(q)\right|^2 = \frac{4\pi}{Z^2(2J_i+1)}\left|\sum_{T=0,1}(-1)^{T_f-T_{zf}}\begin{pmatrix} T_f & T & T_i \\ -T_{Z_f} & 0 & T_{Z_i}\end{pmatrix}\left\langle f \left\| \hat{T}_{JT}^L(q) \right\| i\right\rangle\right|^2 \left|F_{cm}(q)\right|^2 \left|F_{fs}(q)\right|^2$$

(12)

T is constrained through the subsequent select rule:

$$|T_f - T_i| \le T \le T_f + T_i \qquad (12)$$

and $T_Z = \frac{Z-N}{2}$. The platform $\begin{pmatrix} \end{pmatrix}$ in Eq. (12) is the 3 – j symbol and decreased matrix. The configuration of mixing and other components within the spin and isospin space of the longitudinal operator between the last and first plurality of particles states of the structure can be expressed as a function of the One-Body Density Matrix (OBDM) components that are produced by the longitudinal operator's single particle matrix elements [17], i.e.

$$\langle f \| |\hat{T}_{JT}^L| \| i\rangle = \sum_{a,b} OBDM^{JT}(i,f,J,a,b)\ \langle b \| |\hat{T}_{JT}^L| \| a\rangle \qquad (13)$$

Additionally, the longitudinal operator's numerous particle-reduced matrix components, include two components: one for the model space and the other for the core. polarization matrix component [18]:

$$\langle f\| \hat{T}_J^L(\tau_Z,q)\|i\rangle = \left\langle f\left\|\hat{T}_J^{ms L}(\tau_Z,q)\right\| i\right\rangle + \left\langle f\left\|\hat{T}_J^{cor L}(\tau_Z,q)\right\| i\right\rangle \qquad (14)$$

which the model space matrix component in Eq. (13) possesses the shape.

$$\left\langle f\left\|\hat{T}_J^{ms L}(\tau_Z,q)\right\| i\right\rangle = e_i\int_0^\infty drr^2 j_J(qr)\rho^{ms}_{J,\tau_Z}(i,f,r) \qquad (15)$$

The model space transition-density is $\rho^{ms}_J(i,f,r)$. This sum is calculated as the product of the OBDM and the one-particle matrix components, and it is denoted by [18]:

$$\rho^{ms}_{J,\tau_Z}(i,f,r) = \sum_{jj'(ms)}^{ms} OBDM(i,f,J,j,j',\tau_z)\ \langle j\|Y_J\|j'\rangle R_{nl}(r)\ R_{n'l'}(r) \qquad (16)$$

The core-polarization matrix component in Eq. (15) assumes the subsequent shape [14, 15]:

$$\left\langle f\left\|\hat{T}_J^{cor L}(\tau_Z,q)\right\| i\right\rangle = e_i\int_0^\infty dr\, r^2 j_J(qr)\rho^{core}_J(i,f,r). \qquad (17)$$

where ρ^{core}_J is the core-polarization transformation density, which is contingent upon the model utilized for core polarization. The objective is to capture the core-polarization taking implications into account. The group modes of nuclei are described by the model

space and the core-polarization transformation density, which is supplemented through the transition density. The overall density of transitions is calculated as:

$$\rho_{J\tau_z}(i,f,\mathrm{r}) = \overset{ms}{\rho}_{J\tau_z}(i,f,\mathrm{r}) + \overset{core}{\rho}_{J\tau_z}(i,f,\mathrm{r}) \quad \textbf{(18)}$$

The γ-transition and the excited state of nuclei through electron scattering are described using the Tassie model. It is the multipole analysis of inelastic scattering. This model is limited to the standard liquid drop model when a uniform charge distribution is assumed. The Tassie Model is an attempt to develop a model that is more elastic and can be modified to accommodate a non-uniform charge and mass distribution of density. The density of the core-polarization transformation is contingent upon the nucleus's ground state charge density, as per this model. The ground charge density is expressed according to the two-body charge-density distribution across every occupied shell, which includes the core, Within this task. The core polarization transition density is determined by the Tassie form, as per the collective modes of nuclei [19]:

$$\rho^{\mathrm{core}}_{\mathrm{Jt_z}}(\mathrm{i,f,r}) = \mathrm{N}\frac{1}{2}(1+\tau_z)\mathrm{r}^{\mathrm{J}-1}\frac{\mathrm{d}\rho_o(\mathrm{i,f,r})}{\mathrm{dr}} \quad (\textbf{19})$$

During which is the constant of proportionality and the base state 2-body distribution of charge density, shown in Eq. (6). In this formulation, the Coulomb form factor is as follows:

$$F_J^L(q) = \sqrt{\frac{4\pi}{2J_i+1}}\ \frac{1}{Z}\left\{\int_0^\infty r^2 j_J(qr)\,\rho_J^{ms}(i,f,r)\ dr + N\int_0^\infty dr r^2\, j_J(qr) r^{J-1}\ \frac{d\rho_o(i,f,r)}{dr}\right\} F_{cm}(q)\ F_{fs}(q) \quad (\textbf{20})$$

The radial integral $\int_0^\infty \mathrm{dr}\,\mathrm{r}^{\mathrm{J}+1}\mathrm{j_J(qr)}\frac{\mathrm{d}\rho_o(\mathrm{i,f,r})}{\mathrm{dr}}$ can be written as:-

$$\int_0^\infty \frac{\mathrm{d}}{\mathrm{dr}}\{\mathrm{r}^{\mathrm{J}+1}\mathrm{j_J(qr)}\rho_o(\mathrm{i,f,r})\}\mathrm{dr} - \int_0^\infty \mathrm{dr}\,(\mathrm{J}+1)\mathrm{r}^{\mathrm{J}}\mathrm{j_J(qr)}\rho_o(\mathrm{i,f,r}) - \int_0^\infty \mathrm{dr}\mathrm{r}^{\mathrm{J}+1}\frac{\mathrm{d}}{\mathrm{dr}}\mathrm{j_J(qr)}\rho_o(\mathrm{i,f,r}) \quad (\textbf{21})$$

in which the initial term is 0, the 2nd and 3ed terms are joined as:

$$-\mathrm{q}\int_0^\infty \mathrm{dr}\mathrm{r}^{\mathrm{J}+1}\rho_o(\mathrm{i,f,r})\left[\frac{\mathrm{d}}{\mathrm{d(qr)}}+\frac{\mathrm{J}+1}{\mathrm{qr}}\right]\mathrm{j_J(qr)} \quad (\textbf{22})$$

Based on the recurssion link of the spherical Bessel function:

$$\left[\frac{\mathrm{d}}{\mathrm{d(qr)}}+\frac{\mathrm{J}+1}{\mathrm{qr}}\right]\mathrm{j_J(qr)} = \mathrm{j_{J-1}(qr)} \quad (\textbf{23})$$

$$\therefore \int_0^{\infty} \mathrm{dr}\ \mathrm{r}^{\mathrm{J}+1}\mathrm{j}_{\mathrm{J}}(\mathrm{qr})\frac{\mathrm{d}\rho_{\mathrm{o}}(\mathrm{i},\mathrm{f},\mathrm{r})}{\mathrm{dr}} = -\mathrm{q}\int_0^{\infty}\mathrm{drr}^{\mathrm{J}+1}\mathrm{j}_{\mathrm{J}-1}(\mathrm{qr})\,\rho_{\mathrm{o}}(\mathrm{i},\mathrm{f},\mathrm{r}) \qquad (\mathbf{24})$$

Therefore, the form factor is as follows:

$$F_J^L(q) = \left(\frac{4\pi}{2J_i+1}\right)^{1/2}\frac{1}{Z}\left\{\int_0^{\infty}\mathrm{r}^2 j_J(qr)\,\rho_{Jt_z}^{ms}\,dr - \mathrm{N}q\int_0^{\infty}dr\,\mathrm{r}^{J+1}\rho_o(i,f,r)\,j_{J-1}(qr)\right\}F_{cm}(q)\,F_{fs}(q) \qquad \mathbf{(25)}$$

The unchanging of proportionality N may be identified by evaluating the form factor at q=k, resulting in the following:

$$\mathrm{N} = \frac{\int_0^{\infty}\mathrm{drr}^2\mathrm{j}_{\mathrm{J}}(\mathrm{kr})\rho_{\mathrm{Jt_Z}}^{\mathrm{ms}}(\mathrm{i},\mathrm{f},\mathrm{r}) - \mathrm{F}_{\mathrm{J}}^{\mathrm{L}}(\mathrm{k})\mathrm{Z}\sqrt{\frac{2\mathrm{J_i}+1}{4\pi}}}{\mathrm{k}\int_0^{\infty}\mathrm{drr}^{\mathrm{J}+1}\rho_{\mathrm{o}}(\mathrm{i},\mathrm{f},\mathrm{r})\mathrm{j}_{\mathrm{J}-1}(\mathrm{kr})} \qquad (\mathbf{26})$$

$\mathrm{B(CJ)} = \frac{[(2\mathrm{J}+1)!!]^2\mathrm{Z}^2\ \mathrm{e}^2}{4\pi\ \mathrm{k}^{2\mathrm{J}}}\left|\mathrm{F}_{\mathrm{J}}^{\mathrm{L}}(\mathrm{k})\right|^2$, at the photon's collision point(q=k), transitional amplitude *B(CJ)* is correlated with its form factor.

$$\mathrm{N} = \frac{\int_0^{\infty}\mathrm{drr}^2\mathrm{j}_{\mathrm{J}}(\mathrm{kr})\rho_{\mathrm{Jt_z}}^{\mathrm{ms}}(\mathrm{i,f,r}) - \sqrt{\frac{(2\mathrm{J_i}+1)\mathrm{B(CJ)}}{(2\mathrm{J}+1)!!}}\mathrm{k}^{\mathrm{J}}}{\mathrm{k}\int_0^{\infty}\mathrm{drr}^{\mathrm{J}+1}\rho_{\mathrm{o}}(\mathrm{i,f,r})\mathrm{j}_{\mathrm{J}-1}(\mathrm{kr})} \qquad (\mathbf{27})$$

The coefficient of proportionality for open (closed) shell nuclei can be established by incorporating the determined (observed) measure of the reduced transitional amplitude B(CJ) through Eq. (28).

3. Results and Discussion

Figs. 1 and 2 illustrate the ground state charge density distributions (in fm^{-3}) in relation to r (in fm) for ^{20}Ne and ^{24}Mg nuclei. Table 1 contains all the parameters necessary for the calculations including the dimension parameter of the harmonic oscillator (b), the occupancy probabilities ($\eta_{n\ell j}$) of the states. Figs. 1 and 2 display the charge density distribution. The blue dashed line represents the one-body charge density distribution without correction; depending on Eq. (1), the solid blue line is the two-body charge density distribution and the black dotted-symbol line is the experimental data [20] in unit (nucleon. fm^{-3}).

From Figs. 1 and 2, it can be noted that the theoretical results are in good agreement with the experimental results concerning the two body charge density distribution, for the region 0.5 < r <2.5, we expound differ the one-body charge density distribution of charge density and two- body charge density distribution with the experimental data; the solid blue line indicates good agreement with experimental data for this region. The calculated elastic electron scattering form factors F(q) in Figs. 3 and 4, the estimated F(q)'s contrasted to those of observational data for ^{20}Ne and ^{24}Mg nuclei, where the blue dashed line is elastic form factors without correction using Eqs. (1) and (10); the solid blue line is the two-body elastic form factors with the correction using Eqs. (6) and (10); the black dotted- symbol line is the experimental data. In these figures, the calculated F(q)'s are plotted as a function of q, as shown in Figs. 3 and 4. The elastic form factor for one-body charge density distribution is not matching, on the other side, it was noted that when utilizing the two-body distribution of charge density,

the second diffraction appeared in value q = 2.4, which is an approach to the experimental data.

Table 1: The variables employed in the calculations of the current study for each investigated nuclei.

Nuclei	**^{20}Ne**	**^{24}Mg**
b	1.77	1.85
$\alpha^2\,(fm^{-2})$	0.36	0.34
$\eta_{1s_{1/2}}$	1	1
$\eta_{1p_{3/2}}$	1	1
$\eta_{1p_{1/2}}$	1	1
$\eta_{1d_{5/2}}$	0.16667	0.5
$\eta_{2s_{1/2}}$	0.5	0.5
$\langle r^2\rangle^{1/2}_{\text{theo.}}$	3.027	3.125
$\langle r^2\rangle^{1/2}_{\text{exp.}}$[15]	3.005	3.020

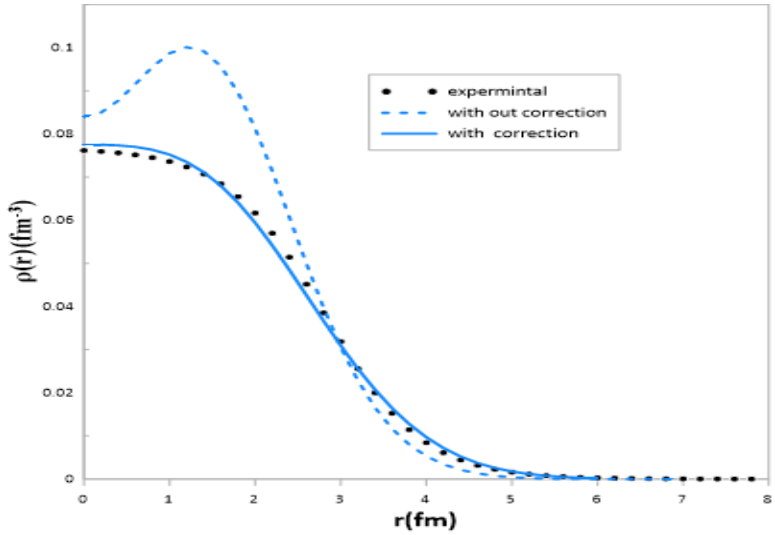

Figure 1: The charge density distribution for ^{20}Ne nucleus.

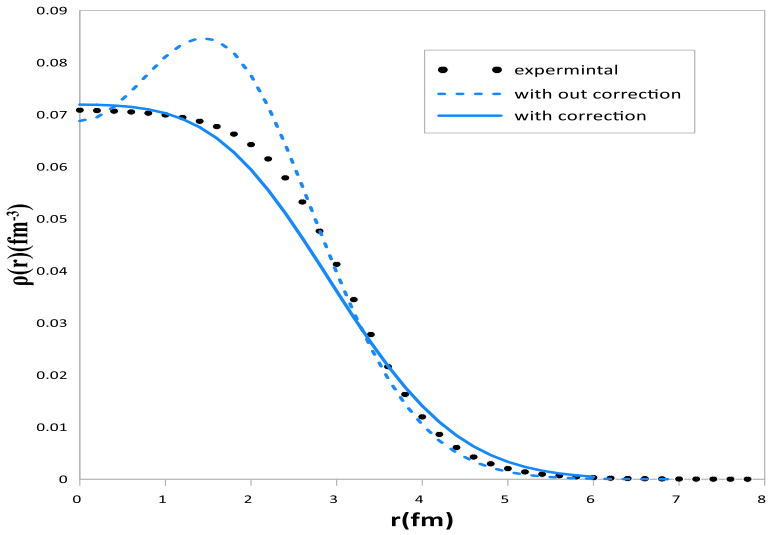

Figure 2: The charge density distribution for ^{24}Mg nucleus.

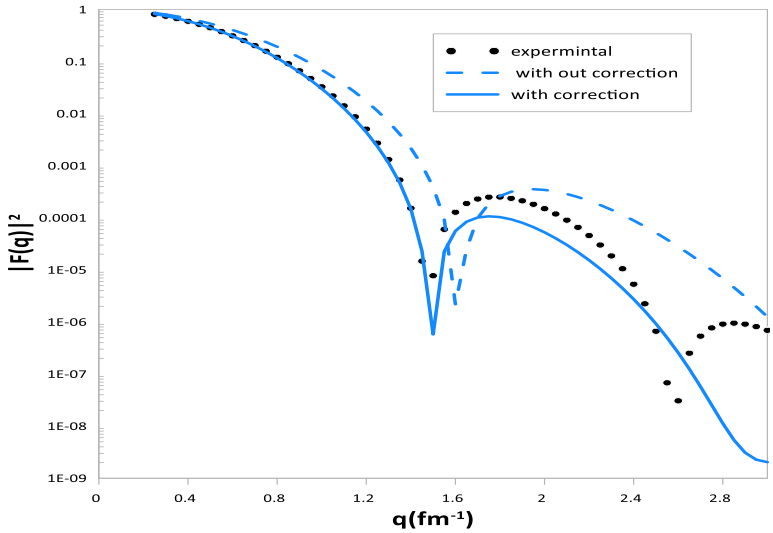

Figure 3: The elastic form factors for ^{20}Ne nucleus.

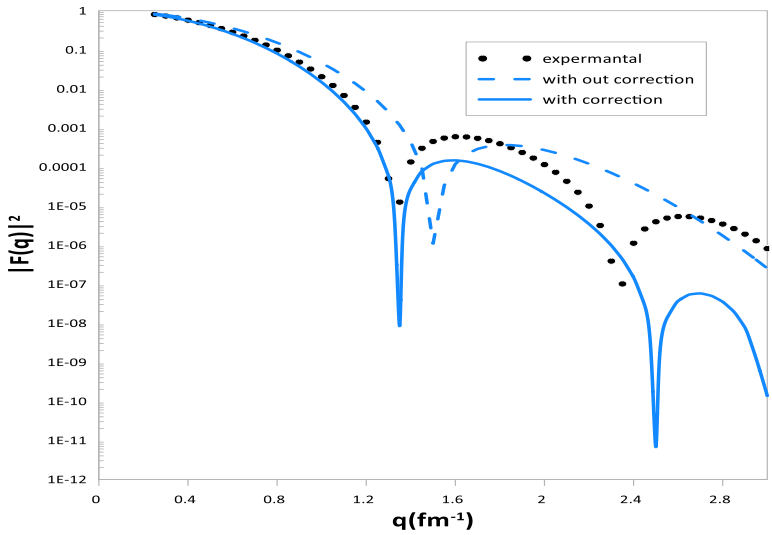

Figure 4: The elastic form factors for ^{24}Mg nucleus.

A formula for the transfer charge density, Eq. (19), was employed to determine the inelastic longitudinal electron scattering form factors F(q). The OXBASH code was used to calculate the OBDM components necessary for the calculations of the form factors of open shell nuclei, resulting in the model space transfer density being determined by Eq. (17) [21] using the interaction matrix elements of USDB (Universal sd-shell B) for 2s-1d shell nuclei [22]. The theoretical determination of the factor N is not indicative of an adjustable parameter. Within this section, the longitudinal C2 form factors that were computed are illustrated in relation to the momentum transfer (q) for the transitions, $0^+ \rightarrow 2^+$ with an observed Ex=1.63MeV [23] and experimental value of B(C2) =278.3 e2.fm4 in ^{20}Ne, with an observed Ex=1.37MeV [23] and experimental value of B(C2) = 404.7 e2.fm4 in ^{24}Mg. In Figs. 5 and 6, the blue dashed curves represent the influence of the model space, and these are adjusted for configuration mixing. The blue dash-dotted curves symbolize the core polarization investment determined by Eq. (20), which is adjusted for the effect of two bodies. The blue solid line is the overall investment, which is calculated by combining the model space and the core polarization impacts determined by Eq. (21). The black dotted-symbol line represents the experimental data. The results shown here demonstrate that the experimental data cannot be replicated by the model space's contributions, as it

understates the data for every momentum transition amounts. When the model space (the solid curves) as well as the effect of core polarization are considered, the longitudinal C2 form factors are improved, resulting in the calculated outcomes being in an acceptable representation of the experimental data for every value of momentum transition q.

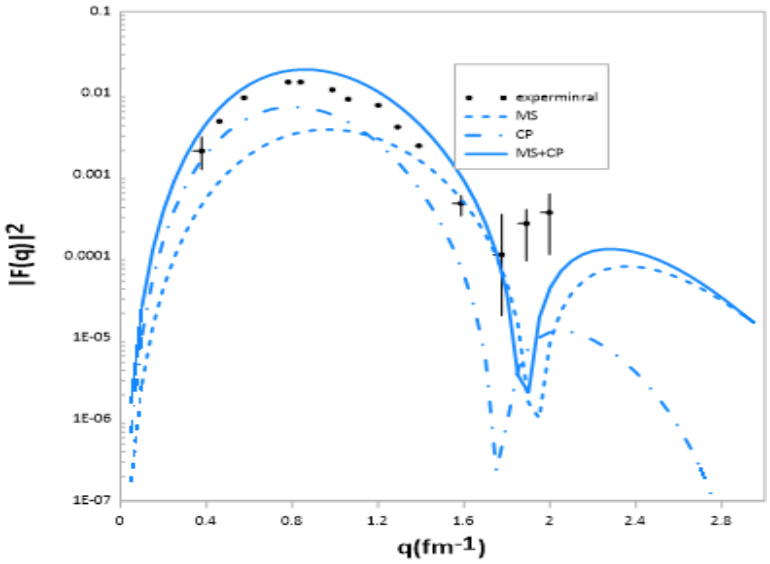

Figure 5: Inelastic longitudinal C2 form factors for ^{20}Ne nucleus.

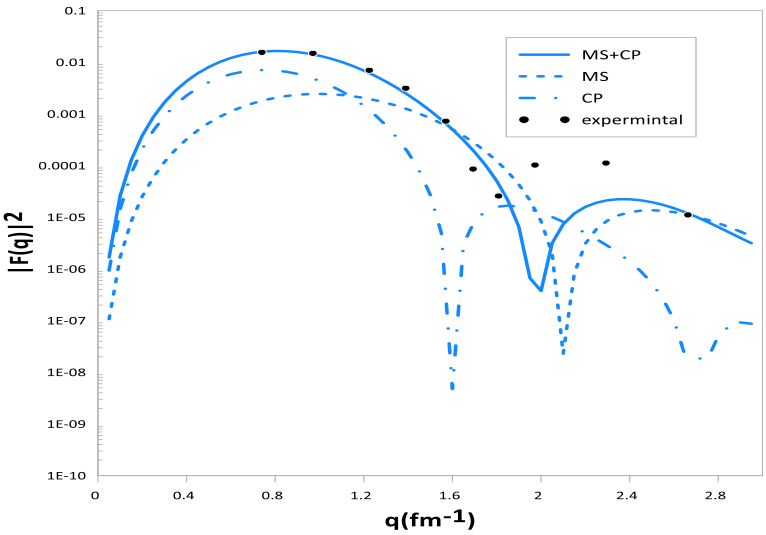

Figure 6: Inelastic longitudinal C2 form factors for ^{24}Mg nucleus.

The graphs shown in Figs. 7 and 8 illustrate the inelastic longitudinal C4 form factors of ^{20}Ne and ^{24}Mg nuclei, respectively. The computed longitudinal C4 form factors are depicted in relation to the momentum transfer q for the transitions in ^{20}Ne and ^{24}Mg with observed excitation energies of 4.25MeV and 6.1MeV, respectively. The experimental B(C4) of the above nuclei are 32500 and 36000 [e^2fm^4], respectively [23-25]. In these figures, the blue-dashed shapes symbolize the influence of the model space, which is adjusted for configuration mixing. The blue dash-dotted shape symbolizes the core polarization investment, which is adjusted to the effect of two bodies. The blue-solid line is the overall investment, calculated by combining the model space and the core polarization impacts. The black dotted-symbol line is the experimental data. These graphs demonstrate that the model space cannot accurate explain the entire area of momentum transfer with the experimental data. However, the

outcomes of the longitudinal C4 form factors become logical and consistent with the experimental data throughout the entire area of momentum transfer "q", as evidenced by the solid curves in these graphs.

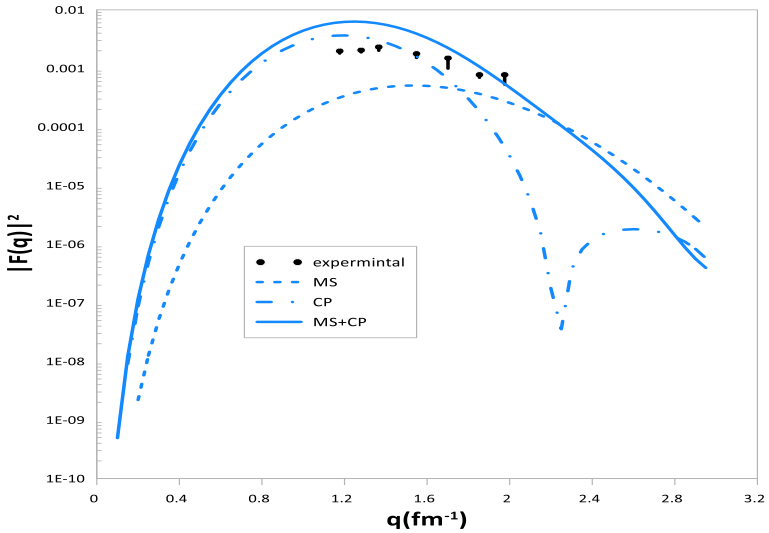

Figure 7: Inelastic longitudinal C4 form factors for ^{20}Ne nucleus.

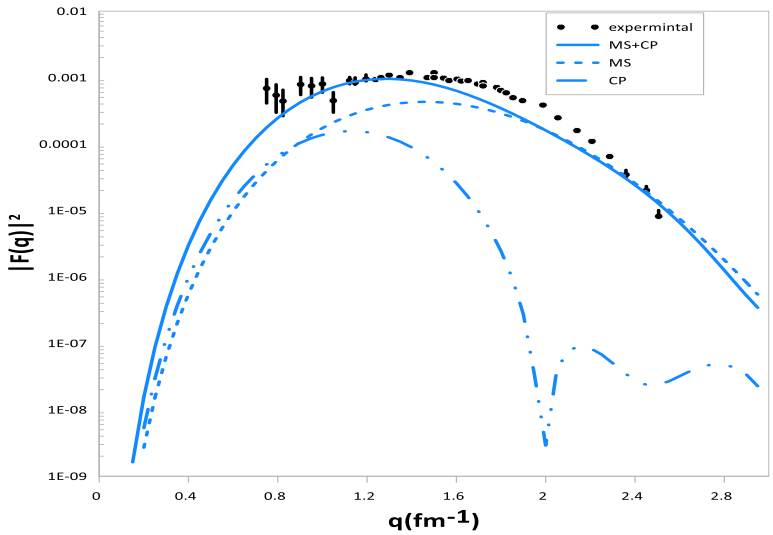

Figure 8: Inelastic longitudinal C4 form factors for ^{24}Mg nucleus.

4. Conclusions

1. Considering the effects of the center of mass and Pauli pair correlation functions and higher occupation probabilities generally, it is crucial to achieve a high degree of alignment between the estimates of charge density distributions with all of the experimental data of ^{20}Ne and ^{24}Mg nuclei.
2. The fixed characteristics and energy levels can be accurately described by the sd-shell models; however, they are less effective in characterizing dynamical characteristics, including the rates of C2 and C4 transitions and the form factors of electron scattering.
3. The core-polarization impacts improve the form factors and bring the mathematical predictions of the longitudinal form factors closer to the experimental data in the C2 and C4 transitions.

Conflict of Interest

The authors declare no conflict of interest.

References

1. T. De Forest Jr and J. D. Walecka, Adv. Phys. **15**, 1 (1966). DOI: 10.1080/00018736600101254.
2. J. D. Walecka, Nucl. Phys. A **574**, 271 (1994). DOI: 10.1016/0375-9474(94)90050-7.
3. J. Hoppe, C. Drischler, R. J. Furnstahl, K. Hebeler, and A. Schwenk, Phys. Rev. C **96**, 054002 (2017). DOI: 10.1103/PhysRevC.96.054002.
4. R. A. Radhi, A. A. Alzubadi, and E. M. Rashed, Nucl. Phys. A **947**, 12 (2016). DOI: 10.1016/j.nuclphysa.2015.12.002.
5. L. A. Mahmood and G. N. Flaiyh, Iraqi J. Sci. **57**, 1742 (2016).
6. L. A. Mahmood, Iraqi J. Phys. **14**, 129 (2016).
7. P. Sarriguren, D. Merino, O. Moreno, E. Moya De Guerra, D. N. Kadrev, A. N. Antonov, and M. K. Gaidarov, Phys. Rev. C **99**, 034325 (2019). DOI: 10.1103/PhysRevC.99.034325.
8. Iraqi J. Sci. **65**, 1357 (2024). DOI: 10.24996/ijs.2024.65.3.16.
9. G. N. Flaiyh and F. I. Sharrad, Iran J. Sci. Tech. Trans. Sci. **42**, 2323 (2018). DOI: 10.1007/s40995-017-0160-x.
10. J. C. Bergstrom, S. B. Kowalski, and R. Neuhausen, Phys. Rev. C **25**, 1156 (1982). DOI: 10.1103/PhysRevC.25.1156.
11. B. A. Brown, B. H. Wildenthal, C. F. Williamson, F. N. Rad, S. Kowalski, H. Crannell, and J. T. O'brien, Phys. Rev. C **32**, 1127 (1985). DOI: 10.1103/PhysRevC.32.1127.
12. I. Ahmad, J. Phys. G: Nucl. Part. Phys. **20**, 507 (1994). DOI: 10.1088/0954-3899/20/3/011.
13. I. Ahmad and J. P. Auger, Nucl. Phys. A **352**, 425 (1981). DOI: 10.1016/0375-9474(81)90421-8.
14. H. G. Benson and B. H. Flowers, Nucl. Phys. A **126**, 305 (1969). DOI: 10.1016/0375-9474(69)90468-0.
15. J. D. Walecka, *Electron Scattering for Nuclear and Nucleon Structure* (Cambridge, Cambridge University Press, 2002).
16. T. W. Donnelly and I. Sick, Rev. Mod. Phys. **56**, 461 (1984). DOI: 10.1103/RevModPhys.56.461.
17. M. Sakakura, J. Japan Phys. Soci. **34**, 525 (1979). DOI: 10.11316/butsuri1946.34.6.525_2.
18. B. A. Brown, R. Radhi, and B. H. Wildenthal, Phys. Rep. **101**, 313 (1983). DOI: 10.1016/0370-1573(83)90001-7.
19. L. Tassie, Australian J. Phys. **9**, 407 (1956). DOI: 10.1071/PH560407.
20. H. De Vries, C. W. De Jager, and C. De Vries, Atomic Data and Nuclear Data Tables **36**, 495 (1987). DOI: 10.1016/0092-640X(87)90013-1.
21. B. Brown, A. Etchegoyen, N. Godwin, W. Rae, W. Richter, W. Ormand, E. Warburton, J. Winfield, L. Zhao, and C. Zimmerman, *MSU-NSCL report number 1289* (2005).
22. B. A. Brown and W. A. Richter, Phys. Rev. C **74**, 034315 (2006). DOI: 10.1103/PhysRevC.74.034315.
23. G. C. Li, M. R. Yearian, and I. Sick, Phys. Rev. C **9**, 1861 (1974). DOI: 10.1103/PhysRevC.9.1861.
24. K. Amos and C. Steward, Phys. Rev. C **41**, 335 (1990). DOI: 10.1103/PhysRevC.41.335.
25. G. Fricke, C. Bernhardt, K. Heilig, L. A. Schaller, L. Schellenberg, E. B. Shera, and C. W. Dejager, Atomic Data and Nuclear Data Tables **60**, 177 (1995). DOI: 10.1006/adnd.1995.1007.

توزيعات كثافة الشحنة، عوامل التشكل للإستطارة للإلكترونية المرنة والغير مرنة للنوى ^{20}Ne و^{24}Mg

حسين خالد عيسى[1] وغيث نعمة فليح[1]

[1]قسم الفيزياء، كلية العلوم، جامعة بغداد، العراق

الخلاصة

تم حساب توزيعات كثافة الشحنة باستخدام انموذج الطي الذي تم تطبيقه لدراسة تأثير مركز الكتلة واقتران زوج باولي على كثافة الشحنة بالاعتماد على التفاعلات الفعالة بين الجسمين، كصيغة لكثافة الجسمين المطبقة على ^{20}Ne و^{24}Mg. يمكن اشتقاقها من حيث تصحيح الارتباط الزوجي. بالنسبة إلى^{20}Ne و^{24}Mg، ومن خلالها تم حساب عوامل التشكل للإستطارة للإلكترونية المرنة F(q) وجذر متوسط مربع نصف قطر الشحنة $\langle r^2 \rangle^{1/2}$. تم حساب عوامل التشكل الطولية للإستطارة للإلكترونية غير المرنة المرتبطة بانتقالات فضاء البرم النظري T = 0 و$(J_i^\pi \rightarrow J_f^\pi)$ ($0^+ \rightarrow 2^+$) و ($0^+ \rightarrow 4^+$) للنوى ^{20}Ne و^{24}Mg كان مصمما كدالة موجية داخل فضاء النموذج(model space)، والتي تم تحديدها بواسطة المدارات $1d_{5/2}$, $2s_{1/2}$ و$1d_{3/2}$، غير قادرة على إنتاج دالة موجية مقبولة بشكل فعال. أن تأثيرات استقطاب القلب حسبت بالاعتماد على شكل أنموذج Tassie الى جانب الصيغة الرياضية المشتقة لتوزيعات كثافة الشحنة النووية باستخدام انموذج الطي.. لقد وجد بان تأثير استقطاب القلب الذي يمثل نمط تجميعي يكون جوهريا للحصول على توافق جيد بين حسابات الاستطارة الطولية غير المرنة (s'*F(q)*) والقيم العملية لجميع النوى قيد الدراسة.

الكلمات المفتاحية: كثافة الشحنات، تشتت الإلكترونات المرنة، تشتت الإلكترونات غير المرنة، انموذج الطي، انموذج تاسي.